



Sb Additions in Near-Eutectic Sn-Bi Solder Decrease Planar Slip

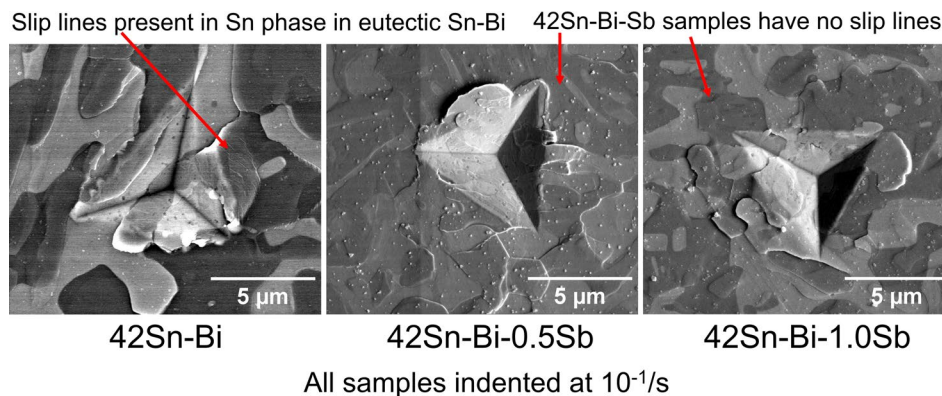
Hannah N. Fowler¹ · Alexandra Loaiza¹ · David F. Bahr¹ · John E. Blendell¹ · Carol A. Handwerker¹

Received: 15 February 2023 / Accepted: 1 August 2023 / Published online: 24 August 2023
© The Minerals, Metals & Materials Society 2023

Abstract

This study examines the changes in strain rate dependence and the deformation behavior of near-eutectic Sn-Bi alloys as a function of Sb concentration using nanoindentation. Alloying near-eutectic Sn-Bi solder with Sb has been shown to increase the strain to failure under tensile and shear conditions in solder ball geometries, with Sb additions remaining in solid solution up to 0.5 wt.% Sb. In this study, the resulting hardness of the three Sb-containing Sn-Bi alloys (Bi-42Sn eutectic, Bi-42Sn-0.5Sb, Bi-42Sn-1.0Sb) exhibits little solid solution hardening at room temperature, and the alloys all exhibited similar strain rate sensitivity behavior, independent of composition for this microstructure. Using nanoindentation and post-indentation microscopy to analyze the deformation behavior of these alloys, the out-of-plane deformation and slip behavior does change with composition. Solute Sb increases the strain hardening behavior at low strains while decreasing planar slip and out-of-plane deformation. The observed changes in deformation modes in this nanoindentation study with the addition of Sb as a solid solution alloy (less slip planarity, more uniform deformation, and more strain hardening) could play a role in previously observed changes in tensile failure modes without the formation of SbSn intermetallic compounds.

Graphical Abstract



Keywords Low-temperature solder · eutectic Sn-Bi · nanoindentation · strain rate sensitivity · slip lines

Introduction

Both the low melting point of eutectic Sn-Bi (139°C) and the high reliability of eutectic Sn-Bi during thermal cycling have resulted in its growing use in consumer electronics. In addition, low-temperature Sn-Bi solders

(LTS) are being used to mitigate heating-induced warpage during reflow and, thus, eliminate warpage-induced manufacturing defects by lowering the reflow temperature by as much as 70°C compared with Sn-3.0Ag-0.5Cu (SAC305). Despite showing high cycles to failure during thermal cycling compared with SAC305, eutectic Sn-Bi underperforms SAC305 in drop-shock testing. The high strain rate dependence of Sn-Bi is a well-recognized phenomenon, and improving the performance of Sn-Bi

✉ Hannah N. Fowler
fowlerh@purdue.edu

¹ Purdue University, West Lafayette, IN, USA

at higher strain rates is crucial to improving the overall reliability of Sn–Bi solder joints.^{1–4}

In tensile tests on bulk alloys, small alloying additions of Cu, Ag, and Sb have been found to increase the strength of Sn–Bi LTS.^{5–9} Additions of Sb have shown the unique effect of improving both the ductility of eutectic Sn–Bi and the strength.^{5,8} This is unexpected since increases in strength are usually associated with decreases in ductility. Sakuyama attributed the high ductility (+40%) and strength with Sb additions to the presence of SnSb intermetallic compound (IMC) particles along the Sn/Bi phase boundary, with the suggestion that Sb solid solution strengthens the Sn phase, and that SnSb IMC particles pin the phase boundary to both prevent the Bi phase from coarsening and provide precipitation hardening.^{5,8}

Prior studies have used a combination of nanoindentation and post-indentation microscopy to identify slip behavior and anomalies on indent surfaces.^{10–14} We use similar methods here to examine how deformation in Sn–Bi LTS is impacted by addition of solute Sb. This study examines whether:

1. the increase in ductility associated with Sb additions to Sn–Bi LTS observed in testing of bulk alloys can be related to nanoindentation behavior of solder joints with different Sb concentrations,
2. the increase in ductility is accompanied by a decrease in the strain rate sensitivity and how that varies with Sb concentration,
3. a change in deformation mechanism due to Sb additions can be observed through examination of the indents.

Experimental Design

Eutectic Sn–Bi solder (Bi–42Sn, by weight) and two custom Sb-containing solder alloys [Bi–42Sn– x Sb ($x=0.5, 1$)] from Scientific Alloys Corporation were obtained in the form of 500- μ m solder spheres. The Sb-containing alloy compositions were confirmed by inductively coupled plasma mass spectrometry (ICP-MS) to fall within the expected range of the requested Bi–42Sn– x Sb ($x=0.5, 1$) with ± 1.3 wt.% Sn, ± 0.1 wt.% Sb.¹⁵ The solder spheres were hand-placed onto flux-coated, 730- μ m-diameter Cu pads coated with an organic surface preservative (OSP) finish and reflowed (melted and solidified) in a DDM Novastar GF-12HC-HT three-zone tabletop reflow oven with a peak oven temperature of 180°C. The alloys remained above the liquidus temperature (139°C) for 90 seconds, and the solder was cooled via natural cooling in air. At 180°C there is some solubility of Cu in molten Sn–Bi eutectic, estimated using ThermoCalc to be 0.03 wt.% Cu. Thus, all the solder samples have a small amount of Cu dissolution from the substrate, as also indicated by previous measurements of an increase in yield strength.¹⁶ Samples were prepared as sandwich joints, with printed circuit board/solder balls reflowed once, then reflowed, and a second circuit board attached using a second reflow. The solder joints were then mounted in room-temperature epoxy, cross sectioned, and polished to a 0.05- μ m diamond finish for nanoindentation and microstructural analysis.

All the Sn–Bi solder alloys have a eutectic lamellar structure in between β -Sn dendrites as shown in the representative microstructures in Fig. 1. The Sn dendrites have Bi precipitates throughout. The small amount of Cu dissolution into the solder results in a thin Cu_6Sn_5 intermetallic (IMC) layer between the Cu substrate and the solder. This IMC

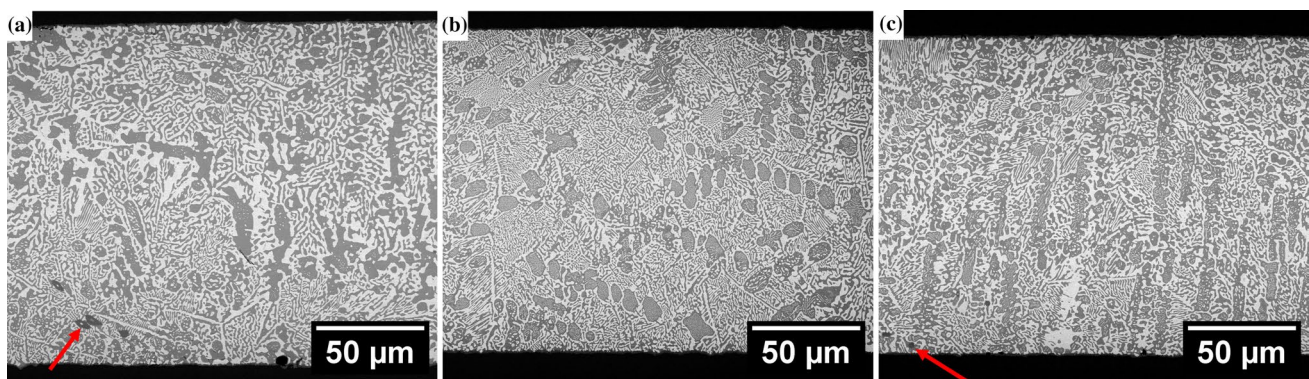


Fig. 1 Representative backscatter SEM images of (a) Bi–42Sn, (b) Bi–42Sn–0.5Sb, and (c) Bi–42Sn–1Sb on an OSP/Cu substrate. Bi is the bright white phase, Sn is the gray phase, and the Cu substrate is the black edge on the top and bottom of the images. The arrows indi-

cate the dark gray Cu_6Sn_5 IMC particles in the lower left corner of (a) and (b). These particles are distributed throughout the solder joint in all the tested alloys in addition to a Cu_6Sn_5 IMC layer between the Cu substrate and the solder.

layer was avoided during nanoindentation. There are also Cu_6Sn_5 IMC particles throughout the solder, seen further away from the IMC layer. Small SnSb IMC particles ranging from 0.5 to 1 μm were observed throughout the Bi-42Sn-1Sb solder as reported in our previous paper.¹⁵

The cross-sectioned solder joints were indented with a Hysitron Triboindenter 950 at three different constant indentation strain rates: $10^{-3}/\text{s}$, $10^{-2}/\text{s}$, and $10^{-1}/\text{s}$ (0.001, 0.01, and 0.1 s^{-1}), using the method described by Lucas et al.¹⁷ A Berkovich indenter tip was used to indent the samples at a constant strain rate to a maximum load of 5000 μN (5 mN). At the end of the loading segment, a constant load was held for 60 s, then the load was removed rapidly. Each indent impression was large enough to encompass multiple phases and provide bulk material properties. By indenting the cross section of the sample, we ensure sampling a region which is effectively semi-infinite in depth relative to the size of the indentation impression.

The Sn phase in eutectic Sn-Bi tends to have higher hardness values during nanoindentation due to the Bi in solid solution in the Sn phase, while the Bi phase with low Sn solubility behaves similarly to pure Bi. This is likely the case in the Sb-containing system as well.^{18–20} Three tests were done at each strain rate for each alloy. After the samples were indented, each indent was imaged using scanning electron microscopy (SEM) to examine the surface for evidence of the local deformation.

Results and Discussion

Examining the load–depth behavior of indentations into soft, creeping solids allows a general understanding of the viscoplastic behavior of these solder alloys. The representative load–depth curves in Fig. 2 show that applied strain rate

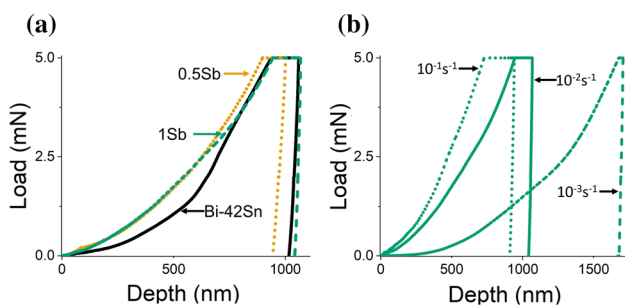


Fig. 2 (a) Representative load–depth curves for each alloy (Bi-42Sn, Bi-42Sn-0.5Sb, and Bi-42Sn-1.0Sb) at loading rates of 10^{-2} s^{-1} . There is no significant variation between the load–depth curves at the same strain rate. (b) Typical load–depth curves for Bi-42Sn-1.0Sb at the three different strain rates (10^{-3} , 10^{-2} , 10^{-1} s^{-1}). As the strain rate increases, the maximum depth decreases, indicating a significant increase in hardness.

impacts hardness more than compositional effects at a single strain rate. See Supplementary 1 for all the load–depth curves. Load–depth curves made with the same tip which are “steeper” (shallower penetration depth for a given load) correspond to a higher hardness (load per projected contact area). Figure 2a shows a constant strain rate indentation at 10^{-2} s^{-1} for each alloy; in general, the depth of each indentation at a given load is similar between these three alloys, suggesting hardness is not dramatically impacted by solute composition at these relatively low strain rates and dilute Sb concentrations. A representative sample of load–depth curves for the 1 wt.% Sb alloy, shown in Fig. 2b, demonstrates that hardness increases as strain rate increases; this effect is consistent in all three alloys in this study. While there are some differences in the shapes of the load–depth curves from alloy to alloy (such as low load pop-in events, or slight changes in shape indicative of potential strain hardening variations as the tip transitions from spherical to pyramidal geometries), adding up to 1 wt.% Sb is not enough to prevent the strain rate-dependent behavior previously observed in bulk tensile tests of eutectic Sn-Bi alloys.^{1–4}

The nominal hardness results for each alloy at the three strain rates are shown in Fig. 3. Hardness was calculated from the maximum applied load and the contact area based on the depth of the indentation determined by the unloading slope in the classical Oliver–Pharr method.²¹ By using a constant hold period, the hardness reported is not at the strain rate at which the loading was performed, and so calculation of a strain rate sensitivity is not appropriate in this case (see Fig. 2b, where the creep at maximum load is a larger fraction of the load–depth curve for higher strain rates). The hardness of the alloys increases with increasing strain rate and are statistically distinct (Fig. 3). There is limited literature on alloys comparable to the alloys in our study. In comparison, Sn-rich solders with Sb addition, such as the Sn-5Sb-1.5Bi alloy tested by Esfandyarpour and Mahmudi, show similar

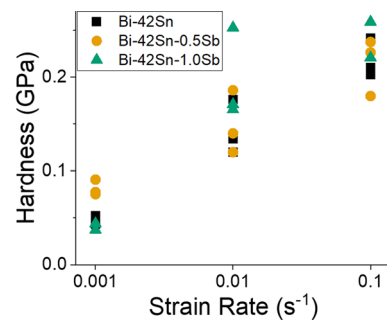


Fig. 3 Hardness values (GPa) for the three solder alloys (Bi-42Sn, Bi-42Sn-0.5Sb, and Bi-42Sn-1.0Sb) loaded at three different strain rates: 0.001, 0.01, and 0.1 s^{-1} . The hardness of the alloys increased with increasing strain rate; the reported hardness is after a 60-s hold period, and so the actual strain rate at the measurement will be less than the loading condition.

strain rate-dependent behavior in tensile tests in the form of increasing ultimate tensile strength (UTS) with increasing strain rate.^{22,23} This trend of increasing hardness with increasing strain rate is also consistent with previous results for eutectic and near-eutectic Sn-Bi alloys.^{1–4,18,19} Our study agrees with the finding that the addition of Sb to Bi-42Sn did not significantly alter the strain rate dependence, in that the Sb-containing samples still followed the trend of increasing hardness with increasing strain rate. This could be attributed to the strain gradient plasticity theory, which explains the increase of geometrically necessary dislocations (GND) with strain rate.^{24,25} However, while strain rate dependency of Sn-Bi in Fig. 3 is unsurprising, the indents themselves show an interesting phenomenon that suggests Sb addition did impact the deformation behavior of Bi-42Sn, which will be discussed next with a discussion of the post-indentation impression morphology.

A representative impression of an indent from each alloy at each strain rate is shown in Fig. 4. The size of the figures was chosen to show the relative size of the plastic zone for each indent. First, as noted in the methods section, all indentations were sufficient to probe multiple grains and phases in the solder alloy, sampling on the order of a dozen grains within the plastic zone of the indentation that extends approximately twice the effective indentation impression radius. Secondly, the out-of-plane deformation around the impression is highest in the Bi-42Sn sample, and relative out-of-plane deformation decreases with increasing Sb additions for all strain rate conditions. Out-of-plane deformation for a given indenter geometry increases with decreased strain hardening coefficients, as seen for multi-phase metallic systems.^{14,26,27} Finally, there is evidence of small cracks and offsets in the

surface topography at the boundary in the post-indentation impressions of deformation near the grain boundaries in all the compositions, but qualitatively more intergranular deformation is present with increasing Sb content, as noted by the arrows in Fig. 4. The Berkovich geometry has a nominal effective strain of 8%, and thus the out-of-plane deformation suggests the macroscopic stress–strain behavior of these alloys would exhibit increases in strain hardening coefficients with increasing Sb solute content because indentations in alloys with increased Sb content exhibited lower amounts of out-of-plane deformation around the indentation.¹⁴ However, it is important to note that bulk tensile testing to determine stress–strain relationships for Bi-42Sn exhibits an onset of necking around 10%,¹ and the vast majority of strain occurs post necking, at strains not probed directly with contact loading methods. The final and most interesting feature of the indentation impressions relates to plastic slip traces around the indentation.

Slip lines on the surface around the indentation impression can be seen in the Bi-42Sn sample for the fastest strain rate tested in this study (0.1 s^{-1}), but these slip lines are not present in any Sb-containing samples at the same strain rate. The slip lines are only present in the Sn phase, and Bi precipitates can impede the motion of the slip lines, as seen in Fig. 4b. The presence of slip lines (which, to form, most likely requires cross-slip processes to occur in the region around the indentation²⁸) suggests that there is stress localization occurring during deformation at the highest strain rate, but this localization is reduced when Sb is added. Therefore, Sb additions to Bi-42Sn lead to more uniform deformation within the Sn phase. Since no surface slip traces were observed in the 0.5 wt.% Sb-containing samples in which no SnSb intermetallics are present, this change in deformation mechanism must

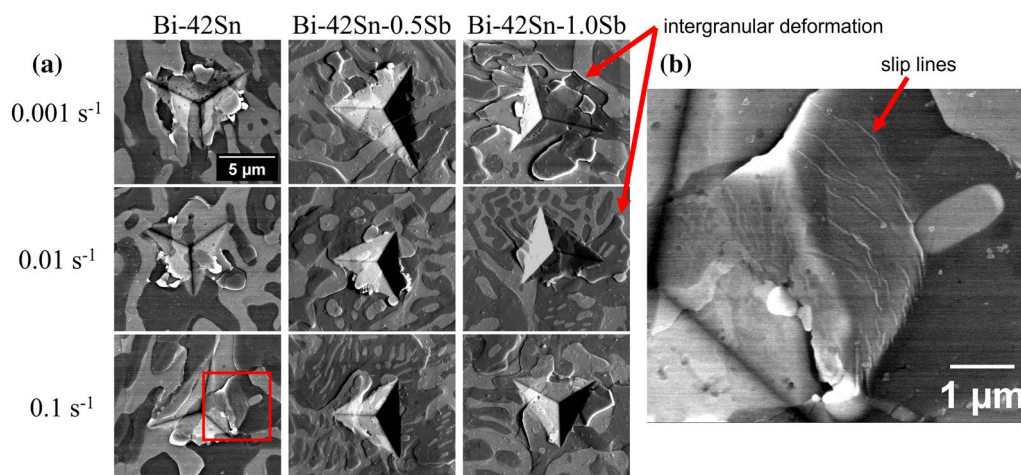


Fig. 4 (a) Representative secondary electron SEM images from each alloy at each strain rate (0.001 , 0.01 , and 0.1 s^{-1}). Bi is the bright phase, and Sn is the dark phase. Slip lines can only be seen in the highlighted Bi-42Sn indent at 0.1 s^{-1} . A higher magnification image

of these slip lines is shown in (b). The image for Bi-42Sn-0.5Sb at 0.1 s^{-1} shows one of the indents made within a Sn dendrite with Bi precipitates. See Supplementary 2 for representative indent locations relative to the overall joint.

be due to the presence of Sb in solid solution within the Sn phase.

Others have previously postulated that Sb addition to Sn-Bi LTS increases the ductility of the alloy while maintaining alloy strength because the SnSb IMC particles pin the phase boundaries and prevent the Bi phase from coarsening.^{5,7–9} However, the transition from localized stresses leading to slip lines present on the surface of the eutectic Sn-Bi sample to the more uniform deformation in the Sn-Bi-0.5Sb and Sn-Bi-1.0Sb LTS alloys is the result of Sb solid solution in the Sn phase since it occurs with and without SnSb IMC particles.^{5,15} In our previous studies, and in the current study, no SnSb IMC particles were found within the 0.5 wt.% Sb samples, and yet the slip lines surrounding indentation impressions have only been observed in the alloy with no Sb.¹⁵ In examining micrographs from the literature, no SnSb IMC particles were apparent in eutectic Sn-Bi-0.5Sb alloys in which the ductility of the alloy increased to 40% elongation in tensile tests compared with 10% for Sn-Bi eutectic, while retaining the strength of the alloy. However, it appears the presence of SnSb particles in the Sn-Bi-0.5Sb alloy and their effects on mechanical behavior were inferred from the microstructure and mechanical behavior of Sn-57.4 wt.% Bi-1 wt.% Sb in which SnSb particles were clearly visible.⁵

We do not mean to imply that nanoindentation and tensile testing to fracture can be compared directly; however, our observations of changes in deformation in the Sn phase with Sb in solid solution suggest more general plasticity in the solid solution could be responsible for previous results showing increased ductility in 0.5 wt.% Sb-containing systems. Several crystal plasticity models of deformation in Sn-based solder have noted the relative sensitivity of the overall deformation to localized slip on particular slip systems; therefore, a lack of stress localization and more uniform deformation could explain how Sb addition to Sn-Bi LTS increases the overall ductility of the alloy.^{29–31} More homogeneous deformation at elevated strain rates would also explain why solute Sb improves the ductility of Sn-Bi LTS. As seen in Fig. 4, the Sb-containing samples show less out-of-plane deformation that reaches further away from the indent, while the eutectic Sn-Bi microstructure shows a higher degree of out-of-plane deformation close to the indent. A change in deformation behavior, with slip planarity decreasing with Sb additions as solid solution within the Sn phase, indicates differences in the relative ease of cross-slip (a necessary mechanism to form slip bands around the surface of the indentation).

Conclusions

The results from this nanoindentation study on Sn-Bi-Sb solder joints match the known trend of increasing hardness with increasing strain rate seen in bulk Sn-Bi LTS alloys.

Solute Sb in Sn-Bi LTS increases the propensity for strain hardening at low (<10%) strains and decreases slip planarity. Increased uniform deformation was observed within the Sn phase of the eutectic alloy with the addition of Sb. The observed changes in deformation modes in this study with adding Sb as a solid solution (less slip planarity, more uniform deformation, and more strain hardening) could play a role in prior observations of changes in tensile failure modes without the formation of SbSn IMCs. Changes in strain hardening and slip planarity could alter the tensile failure modes, but we emphasize that this indentation study is not sufficient to directly predict failure mechanisms in tension.

Supplementary Information The online version contains supplementary material available at <https://doi.org/10.1007/s11664-023-10666-6>.

Acknowledgments This work was supported by the Semiconductor Research Corporation (SRC). We acknowledge additional support from the US Department of Defense [Contract No. W52P1J-22-9-3009]. The views and conclusions contained in this document are those of the authors and should not be interpreted as representing the official policies, either expressed or implied, of the US Department of Defense or the US Government. The US Government is authorized to reproduce and distribute reprints for Government purposes, notwithstanding any copyright notation herein.

Conflict of interest The authors declare that they have no conflict of interest.

References

1. M. McCormack, H.S. Chen, G.W. Kammlott, and S. Jin, Significantly Improved Mechanical Properties of Bi-Sn Solder Alloys by Ag-Doping. *J. Electron. Mater.* 26, 954–958 (1997). <https://doi.org/10.1007/S11664-997-0281-7>.
2. X. Hu, X. Yu, Y. Li, Q. Huang, Y. Liu, and Z. Min, Effect of strain rate on interfacial fracture behaviors of Sn-58Bi/Cu solder joints. *J. Mater. Sci.: Mater. Electron.* 25, 57–64 (2014). <https://doi.org/10.1007/s10854-013-1548-9>.
3. S. Liu, S. McDonald, K. Sweatman, and K. Nogita, The Effects of Precipitation Strengthening and Solid Solution Strengthening on Strain Rate Sensitivity of Lead-Free Solders: Review. *Microelectron. Reliabil.* 84, 170–180 (2018). <https://doi.org/10.1016/j.microrel.2018.03.038>.
4. Z. Zhou, X. Ma, M.B. Zhou, C. Yin, X.P. Zhang, Effect of isothermal aging on mechanical properties and strain rate sensitivity of the eutectic Sn-58Bi solder alloy, in *18th International Conference on Electronic Packaging Technology, ICEPT 2017*, pp 1586–1591. Institute of Electrical and Electronics Engineers Inc. (2017)
5. S. Sakuyama, T. Akamatsu, K. Uenishi, and T. Sato, Effects of a Third Element on Microstructure and Mechanical Properties of Eutectic Sn-Bi Solder. *Trans. Jpn. Inst. Electron. Packag.* 2, 98–103 (2009). <https://doi.org/10.5104/jiepeng.2.98>.
6. Z. Wang, Q.K. Zhang, Y.X. Chen, and Z.L. Song, Influences of Ag and In Alloying on Sn-Bi Eutectic Solder and SnBi/Cu Solder Joints. *J. Mater. Sci.-Mater. Electron.* 30, 18524–18538 (2019). <https://doi.org/10.1007/s10854-019-02206-y>.
7. F. Yang, L. Zhang, Z.-Q. Liu, S.-J. Zhong, J. Ma, and L. Bao, Properties and Microstructures of Sn-Bi-X Lead-Free Solders.

- Adv. Mater. Sci. Eng.* (2016). <https://doi.org/10.1155/2016/9265195>.
8. J.G. Li, X. Ma, M.B. Zhou, X. Ning, X.P. Zhang, Effects of Sb addition on the microstructure and mechanical performance of Sn58Bi based alloys and the solder joints, in *Proceedings - 2018 19th International Conference on Electronic Packaging Technology, ICEPT 2018*. Institute of Electrical and Electronics Engineers Inc., pp. 457–461 (2018)
 9. C. Zhang, S.D. Liu, G.T. Qian, J. Zhou, and F. Xue, Effect of Sb Content on Properties of Sn-Bi Solders. *Trans. Nonferr. Met. Soc. China (Eng. Ed.)* 24, 184–191 (2014). [https://doi.org/10.1016/S1003-6326\(14\)63046-6](https://doi.org/10.1016/S1003-6326(14)63046-6).
 10. K.A. Nibur, and D.F. Bahr, Identifying Slip Systems Around Indentations in FCC Metals. *Scr. Mater.* 49, 1055–1060 (2003). <https://doi.org/10.1016/J.SCRIPTAMAT.2003.08.021>.
 11. Y. Gaillard, C. Tromas, and J. Woignard, Study of the Dislocation Structure Involved in a Nanoindentation Test by Atomic Force Microscopy and Controlled Chemical Etching. *Acta Mater.* 51, 1059–1065 (2003). [https://doi.org/10.1016/S1359-6454\(02\)00509-8](https://doi.org/10.1016/S1359-6454(02)00509-8).
 12. Z. Li, J. Zhang, Y. Zhai, J. Zhang, X. Wang, Z. Zhang, S. Mao, and X. Han, Dynamic Mechanisms of Strengthening and Softening of Coherent twin Boundary via Dislocation Pile-up and Cross-Slip. *Mater. Res. Lett.* 10, 539–546 (2022). <https://doi.org/10.1080/21663831.2022.2065892>.
 13. J. Varillas, J. Očenášek, J. Torner, and J. Alcalá, Unraveling Deformation Mechanisms Around FCC and BCC Nanocontacts Through Slip Trace and Pileup Topography Analyses. *Acta Mater.* 125, 431–441 (2017). <https://doi.org/10.1016/J.ACTAMAT.2016.11.067>.
 14. J.L. Bucaille, S. Stauss, E. Felder, and J. Michler, Determination of Plastic Properties of Metals by Instrumented Indentation Using Different Sharp Indenters. *Acta Mater.* 51, 1663–1678 (2003). [https://doi.org/10.1016/S1359-6454\(02\)00568-2](https://doi.org/10.1016/S1359-6454(02)00568-2).
 15. H.N. Fowler, S.X. Tay, J. Blendell, and C.A. Handwerker, Microalloying Effects of Sb and Ag on the Microstructural Evolution of Eutectic Sn–Bi Alloys. *MRS Adv.* 2023, 1–5 (2023). <https://doi.org/10.1557/S43580-022-00472-3>.
 16. Y. Fan, Y. Wu, T.F. Dale, S.A.P. Lakshminarayana, C.V. Greene, N.U. Badwe, R.F. Aspandiar, J.E. Blendell, G. Subbarayan, and C.A. Handwerker, Influence of Pad Surface Finish on the Microstructure Evolution and Intermetallic Compound Growth in Homogeneous Sn-Bi and Sn-Bi-Ag Solder Interconnects. *J. Electron. Mater.* 50, 6615–6628 (2021). <https://doi.org/10.1007/S11664-021-09256-1>.
 17. B.N. Lucas, and W.C. Oliver, Indentation Power-Law Creep of High-Purity Indium. *Metall. Mater. Trans. A Phys. Metall. Mater. Sci.* 30, 601–610 (1999). <https://doi.org/10.1007/S11661-999-0051-7>.
 18. L. Shen, P. Septiwerdani, and Z. Chen, Elastic Modulus, Hardness and Creep Performance of SnBi Alloys Using Nanoindentation. *Mater. Sci. Eng., A* 558, 253–258 (2012). <https://doi.org/10.1016/j.msea.2012.07.120>.
 19. L. Shen, P. Lu, S. Wang, and Z. Chen, Creep Behaviour of Eutectic SnBi Alloy and Its Constituent Phases Using Nanoindentation Technique. *J. Alloys Compd.* 574, 98–103 (2013). <https://doi.org/10.1016/j.jallcom.2013.04.057>.
 20. F. Wang, A. Luktuke, and N. Chawla, Microstructural Coarsening and Mechanical Properties of Eutectic Sn-58Bi Solder Joint During Aging. *J. Electron. Mater.* 50, 6607–6614 (2021). <https://doi.org/10.1007/S11664-021-09255-2>.
 21. W.C. Oliver, and G.M. Pharr, An Improved Technique for Determining Hardness and Elastic Modulus Using Load and Displacement Sensing Indentation Experiments. *J. Mater. Res.* 7, 1564–1583 (1992). <https://doi.org/10.1557/JMR.1992.1564>.
 22. M.J. Esfandyarpour, and R. Mahmudi, Microstructure and Tensile Behavior of Sn-5Sb Lead-Free Solder Alloy Containing Bi and Cu. *Mater. Sci. Eng., A* 530, 402–410 (2011). <https://doi.org/10.1016/J.MSEA.2011.09.103>.
 23. R. Mahmudi, and S. Mahin-Shirazi, Effect of Sb Addition on the Tensile Deformation Behavior of Lead-Free Sn-3.5Ag Solder Alloy. *Mater. Des.* 32, 5027–5032 (2011). <https://doi.org/10.1016/J.MATDES.2011.05.052>.
 24. W.D. Nix, and H. Gao, Indentation Size Effects in Crystalline Materials: A Law for Strain Gradient Plasticity. *J. Mech. Phys. Solids* 46, 411–425 (1998). [https://doi.org/10.1016/S0022-5096\(97\)00086-0](https://doi.org/10.1016/S0022-5096(97)00086-0).
 25. A.A. Elmustafa, and D.S. Stone, Nanoindentation and the Indentation Size Effect: Kinetics of Deformation and Strain Gradient Plasticity. *J. Mech. Phys. Solids* 51, 357–381 (2003). [https://doi.org/10.1016/S0022-5096\(02\)00033-9](https://doi.org/10.1016/S0022-5096(02)00033-9).
 26. D.F. Bahr, and W.W. Gerberich, Plastic Zone and Pileup Around Large Indentations. *Metall. Mater. Trans. A Phys. Metall. Mater. Sci.* 27, 3793–3800 (1996). <https://doi.org/10.1007/BF02595628>.
 27. R.M. Rahimi, and D.F. Bahr, Individual Phase Deformation and Flow Correlation to Macroscopic Constitutive Properties of DP1180 Steel. *Mater. Sci. Eng., A* 756, 328–335 (2019). <https://doi.org/10.1016/J.MSEA.2019.04.063>.
 28. C. Tromas, J.C. Girard, and J. Woignard, Study by Atomic Force Microscopy of Elementary Deformation Mechanisms Involved in Low Load Indentations in MgO Crystals. *Philos. Mag.* A 80, 2325–2335 (2009). <https://doi.org/10.1080/01418610008216475>.
 29. A. Zamiri, T.R. Bieler, and F. Pourboghra, Anisotropic Crystal Plasticity Finite Element Modeling of the Effect of Crystal Orientation and Solder Joint Geometry on Deformation After Temperature Change. *J. Electron. Mater.* 38, 231–240 (2009). <https://doi.org/10.1007/S11664-008-0595-0>.
 30. P. Darbandi, T.R. Bieler, F. Pourboghra, and T.K. Lee, Crystal Plasticity Finite-Element Analysis of Deformation Behavior in Multiple-Grained Lead-Free Solder Joints. *J. Electron. Mater.* 42, 201–214 (2013). <https://doi.org/10.1007/S11664-012-2339-4>.
 31. P. Darbandi, T.K. Lee, T.R. Bieler, and F. Pourboghra, Crystal Plasticity Finite Element Study of Deformation Behavior in Commonly Observed Microstructures in Lead Free Solder Joints. *Comput Mater Sci* 85, 236–243 (2014). <https://doi.org/10.1016/J.COMMATSCI.2014.01.002>.

Publisher's Note Springer Nature remains neutral with regard to jurisdictional claims in published maps and institutional affiliations.

Springer Nature or its licensor (e.g. a society or other partner) holds exclusive rights to this article under a publishing agreement with the author(s) or other rightsholder(s); author self-archiving of the accepted manuscript version of this article is solely governed by the terms of such publishing agreement and applicable law.